Journal of The Electrochemical Society, **153** (8) A1459-A1465 (2006)
0013-4651/2006/153(8)/A1459/7/$20.00 © The Electrochemical Society

Impedance Simulation of a Li-Ion Battery with Porous Electrodes and Spherical Li^+ Intercalation Particles

R. W. J. M. Huang,[a] Foen Chung,[a,b] and E. M. Kelder[a,*,z]

[a]*Laboratory for Inorganic Chemistry, and* [b]*Physical Chemistry and Molecular Thermodynamics, Delft University of Technology, Julianalaan 136, 2628 BL Delft, The Netherlands*

We present a semimathematical model for the simulation of the impedance spectra of a rechargeable lithium batteries consisting of porous electrodes with spherical Li^+ intercalation particles. The particles are considered to have two distinct homogeneous phases as a result of the intercalation and deintercalation of Li^+ during charge and discharge. The diffusion of Li^+ ions in the two phases and the charge transfer at the solid electrolyte interface (SEI) are described with a mathematical model. The SEI and the electrolyte are modeled using passive electronic elements. First, this model is derived for a single intercalation particle consisting of two different solid phases. This model is then transformed to a continuous model and applied to a single porous electrode, where the sizes of the particles are assumed to have on average two grain sizes where the radii are Gaussian distributions. Finally, this model is further developed to simulate the impedance of a rechargeable lithium-ion battery.
 [DOI: 10.1149/1.2203947]

Manuscript received June 10, 2005; revised manuscript received March 3, 2006. Available electronically June 5, 2006.

In general, aging of dynamic systems is a major concern and finding relevant aging mechanisms is then of vital importance. For batteries, many efforts have been undertaken in order to estimate the calendar life of these systems. In the case of the more recent Li-ion batteries, a lot of work was already performed within the Department of Energy's Advanced Technology Program (DoE-ATP). Electrochemical studies including impedance spectroscopy are widely used for that purpose. Unfortunately, these methods can only provide indirect proof of certain aging mechanisms. Therefore, additional research, such as postmortem analysis, is a prerequisite to determine the most relevant mechanisms that contribute to aging. Subsequently, these aging parameters then should be translated into electrochemical behavior that is monitored with electrochemical equipment. During the last decade, many aging mechanisms have been identified for Li-ion batteries. A wide overview that comprises cathode, anode, electrolyte, and current collectors is given in Ref. 1. The present model uses a transformation of a complex model in the time domain into the frequency domain, which is typically the outcome of impedance spectroscopy. The aging then is introduced via typical aging parameters identified in Ref. 1. For the current calculations, the focus is on the positive electrode, as it has been reported recently that this electrode is the major source for aging.[2-4] The idea is to show the influence of potential sources of degradation on impedance with focus on aging, which may result in reduction of the particle size and changes in the particle size distribution, due for instance, to dissolution of material, and on changes in the solid electrolyte interface that may occur during the lifetime of a battery. Besides, when the system is subject to even small crystallographic changes, the diffusion coefficient may be altered as well.

$LiNiO_2$ and $LiCoO_2$ are well-known compounds for use as positive electrodes in lithium secondary batteries because of their high energy density and very high discharge potential.[5-8] However, it is known that the structures of these materials are metastable and dependent on, for instance, the temperature or number of intercalated Li^+ ions.[9-13] To stabilize the structure and thus favor a good reversibility of the intercalation and deintercalation of Li^+ ions, mixed phases like $Li_xNi_{1-y}Co_yO_2$ are used.[14] For instance, in contrast to $LiNiO_2$, $Li_xNi_{0.8}Co_{0.2}O_2$ has a hexagonally layered structure that does not undergo a phase transition when Li^+ is removed from its lattice site, because the presence of the 20% Co in the $(NiO_2)_n$ slabs hinders the lithium–nickel vacancy ordering mechanism.[15-18] However, according to the results of Saadoune et al.,[15] the unit cell parameters and the Li^+ ionic diffusion coefficient change during the variation of the percentage of intercalated Li^+ ions during the electrochemical cycling. Because many of the commercial batteries today contain layered $LiNi_{0.8}Co_{0.2}O_2$ materials, the work presented here has focused on this material.

In order to incorporate changes in the structure of the electrode compound, which as a result lead to different Li^+ ionic diffusivity, we treat the particles as spheres having two distinct and homogeneous phases in our computer model to simulate the electrochemical impedance spectroscopy (EIS). EIS is a powerful technique to study several aspects in a lithium cell, such as Li^+-ion and electron migration mechanisms, interfacial phenomenon, and failure mechanisms.[19-26] During an EIS experiment, a small perturbing current or voltage is applied to an electrochemical system and the measured response of the system is described as impedance, which is the ratio of voltage to current. Regardless of whether a potential difference or current is applied as signal, the impedance should be the same, because the response of the system is linear.

In the past the impedance response has been described by ideal equivalent-circuits elements, which lead to the difficulty of interpreting the parameters in terms of fundamental properties. Here we model the impedance of a lithium-ion battery using a semimathematical approach. First the impedance response is determined by mathematically solving the diffusion process in the particles. Following the method of Meyers et al. and Srinivasan and Newman,[27-29] we then combine this model with the theory for porous electrodes to describe the impedance of an electrode consisting of spherical particles with two different phases. The method has been further extended by Levi and Aurbach[30] using geometrically inhomogeneous electrodes. Assuming that the electron transport is much faster than the ionic diffusion in the electrolyte, the electrode is simply in series with the electrolyte, described by a resistor in the simulation of the impedance of the cell.

With this cell impedance simulation program we tested the influence of the state of charge, Li^+ diffusion coefficient, thickness of the solid electrolyte interface, and the particle distribution on the impedance of a lithium-ion battery. We concentrated particularly on the positive electrode and therefore, the parameters of the negative electrode and the electrolyte were kept constant in all simulations.

The Mathematical Model

Single spherical particle model.— In order to construct the model for simulating the EIS for a complete cell, the first approach is analyzing the single spherical particle impedance. This then is introduced in an assumed single porous electrode. Finally, the cell impedance is simulated by two of these porous electrodes separated by an electrolyte.

In Fig. 1 a schematic diagram is shown of a spherical Li^+ intercalation particle. The particle consists of two distinct phases denoted by 1 and 2. The radii R_1 and R_2 indicate the borders. The Li^+ self-

* Electrochemical Society Active Member.
z E-mail: e.m.kelder@tnw.tudelft.nl

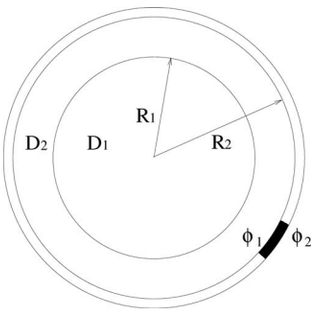

Figure 1. Schematic diagram of a spherical Li^+ intercalation particle consisting of two distinct phases and an SEI. D_1 and D_2 are the Li^+ diffusion coefficient, R_1 and R_2 the radii of the two phases, and Φ_1 and Φ_2 the potential at both ends of the SEI.

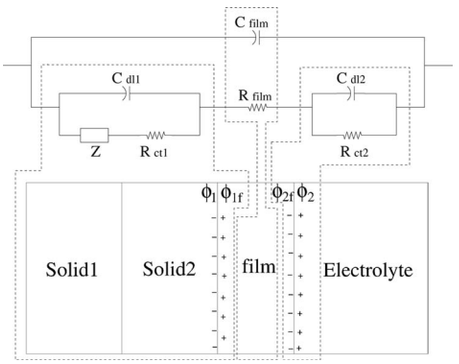

Figure 3. Equivalent-circuit diagram. The relationship with Fig. 2 is marked with dashed lines.

diffusion coefficient in the two phases 1 and 2 are D_1 and D_2, respectively. The spherical particle also contains a solid electrolyte interface (SEI) or film, with Φ_1 and Φ_2 the potential at both ends of the SEI.

In Fig. 2 a detailed picture is displayed of the interfaces along the radius of the spherical particle, and in Fig. 3 is its equivalent-circuit diagram. Also in Fig. 3, the origins of the elements in the equivalent circuit are indicated in the recall of Fig. 2. The diffusion in phases 1 and 2 denoted in Fig. 2 as Solid1 and Solid2 are described mathematically. This gives the component Z in Fig. 3, referred to as the diffusion impedance component, and is described in more detail later on. It is assumed that ionic motion in the SEI or film occurs solely by drift and not via diffusion. From the above consideration, R_{film} is the resistor of the SEI for ionic motion. This gives a resistive current density of i_{film}

$$i_{\text{film}} = \frac{\phi_{1f} - \phi_{2f}}{R_{\text{film}}} \quad [1]$$

The charge separation across the film is described by C_{film}, which then leads to a current density of

$$i_{\text{dl,film}} = C_{\text{film}} \frac{\partial(\phi_1 - \phi_2)}{\partial t} \quad [2]$$

In Eq. 1 and 2, ϕ_{1f}, ϕ_{2f}, ϕ_1, and ϕ_2 are the potentials at the interfaces of the SEI, as indicated in Fig. 2 and 3. The current density due to the charging and discharging of the electrochemical double layer at the inner and outer interface of the SEI is

$$i_{\text{dl1}} = C_{\text{dl1}} \frac{\partial(\phi_1 - \phi_{1f})}{\partial t}$$

$$i_{\text{dl2}} = C_{\text{dl2}} \frac{\partial(\phi_{2f} - \phi_2)}{\partial t} \quad [3]$$

The total current density of the inner interface of the SEI can be written as

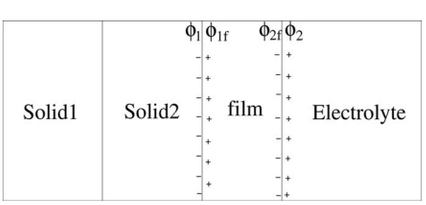

Figure 2. Detailed picture of the interfaces in one dimension along the radius of the spherical intercalation particle.

$$i_{\text{interface}} = i_{\text{faradaic}} + i_{\text{dl1}} \quad [4]$$

where i_{faradaic} is the faradaic current density, which can be related to the potential drop across the interface by the Butler–Volmer equation

$$i_{\text{faradaic}} = i_{o,1}\left[e^{[\alpha_a F/RT(\phi_1 - \phi_{1f} - U)]} - e^{[-\alpha_a F/RT(\phi_1 - \phi_{1f} - U)]}\right] \quad [5]$$

In Eq. 5, U is the open-circuit potential of the charge-transfer reaction, and α_a and α_c are the anodic and cathodic transfer coefficients, respectively, where $\alpha_a + \alpha_c = 1$. $i_{o,1}$ is the exchange-current density, i.e., it can be regarded as the current amplitude in the ac signal, applied during the impedance measurement.

Diffusion impedance component.— The impedance component depends on the migration kinetics of the moving charge carriers. In the two-phase character assumed here, the migration is described by diffusion rather then by drift, because the voltage profile often shows sloppy behavior rather than a flat plateau. Besides, we assume the electronic mobility to be much faster than that of the intercalating Li^+ ions, and therefore, the diffusion of intercalating Li^+ ions in solids 1 and 2 are considered to follow Fick's law. In the time domain the diffusion equations in the two phases are

$$\frac{\partial c_1(r,t)}{\partial t} = \frac{D_1}{r^2}\frac{\partial}{\partial r}\left(r^2 \frac{\partial c_1(r,t)}{\partial r}\right) \quad \text{for } 0 \leq r \leq R_1$$

$$\frac{\partial c_2(r,t)}{\partial t} = \frac{D_2}{r^2}\frac{\partial}{\partial r}\left(r^2 \frac{\partial c_2(r,t)}{\partial r}\right) \quad \text{for } R_1 \leq r \leq R_2 \quad [6]$$

In the frequency domain the diffusion equations can be written as

$$j\omega c_1(r) = \frac{D_1}{r^2}\frac{\partial}{\partial r}\left(r^2 \frac{\partial c_1(r)}{\partial r}\right) \quad \text{for } 0 \leq r \leq R_1$$

$$j\omega c_2(r) = \frac{D_2}{r^2}\frac{\partial}{\partial r}\left(r^2 \frac{\partial c_2(r)}{\partial r}\right) \quad \text{for } R_1 \leq r \leq R_2 \quad [7]$$

Equation 2 can be solved analytically and its general solution yields

$$c_1(r) = b_1 \frac{\sin\left(\sqrt{\frac{-j\omega}{D_1}}r\right)}{r} + b_2 \frac{\cos\left(\sqrt{\frac{-j\omega}{D_1}}r\right)}{r} \quad \text{for } 0 \leq r \leq R_1$$

$$c_2(r) = b_3 \frac{\sin\left(\sqrt{\frac{-j\omega}{D_2}}r\right)}{r} + b_4 \frac{\cos\left(\sqrt{\frac{-j\omega}{D_2}}r\right)}{r} \quad \text{for } R_1 \leq r \leq R_2 \quad [8]$$

Here b_1, b_2, b_3, and b_4 are constants. It can easily be seen that $b_2 = 0$, because $c_1(r = 0)$ has to be finite. b_1, b_3, and b_4 can be determined by the following boundary conditions

$$c_1(R_1) = c_2(R_1)$$

$$\frac{\partial c_1(R_1)}{\partial r} = \frac{\partial c_2(R_1)}{\partial r}$$

$$N_{\text{intercalated}} = \frac{i_{\text{faradaic}}}{F} = -D_2\frac{\partial c_2(R_2)}{\partial r} \quad [9]$$

The first and second boundary conditions are applied because the concentration profile as well as the flux of Li^+ ions have to be continuous at $r = R_1$. At $r = R_2$ the flux has to be equal to the flux of the intercalating Li^+ ions, $N_{\text{intercalated}}$, which is implied by the third boundary condition. Here i_{faradaic} is the faradaic current density at the interface between the SEI and phase 2, and F is Faraday's constant. Linearization of the Butler–Volmer equation (Eq. 5) around open-circuit conditions[27] gives

$$i_{\text{faradaic}} = \frac{i_{o,1}(\alpha_a + \alpha_c)}{RT}\left[\phi_1 - \phi_{1f} - \left(-\frac{\partial U}{\partial c_2}\right)c_2(R_2)\right] \quad [10]$$

Here $\partial U/\partial c_2$ can be related to the first derivative of the charge/discharge curve. In our simulation model the charge/discharge curve is fitted to a 4th degree polynomial, which is a function of the mol fraction (x) of Li^+ ions. From the five parameters a_0, a_1, a_2, a_3, and a_4 of the polynomial we can determine $-[\partial U(x_0)/\partial x]$ as

$$-\frac{\partial U(x_0)}{\partial x} = -4a_4x_0^3 - 3a_3x_0^2 - 2a_2x_0 - a_1 \quad [11]$$

x_0 is determined from the state of charge (SoC) in percentage as $x_0 = [1 - (SOC/100)]$ and $x_0 = SOC/100$ for a positive and negative electrode, respectively. Finally $-[\partial U(x_0)/\partial c_2]$ can be calculated as

$$-\frac{\partial U(x_0)}{\partial c_2} = -\frac{(M_e/\rho_e)}{x_0}\frac{\partial U(x_0)}{\partial x} \quad [12]$$

where M_e is the molar mass and ρ_e is the electrode density.

Now R_{ct1} and the diffusion impedance component Z, as depicted in the equivalent-circuit diagram in Fig. 3, can be defined as

$$R_{ct1} = \frac{RT}{i_{o,1}(\alpha_a + \alpha_c)F}$$

$$Z = \frac{\left(-\frac{\partial U}{\partial c_2}c_2(R_2)\right)}{i_{\text{faradaic}}} \quad [13]$$

so that, with Eq. 10, the faradaic impedance is

$$Z_{\text{faradaic}} = \frac{(\phi_1 - \phi_{1f})}{i_{\text{faradaic}}} = (R_{ct1} + Z) \quad [14]$$

To simplify the simulation program codes, the impedance term Z is defined as

$$Z = \frac{R_{\text{part}}}{Y_s} \quad [15]$$

Solving the constants b_1, b_3, and b_4 in Eq. 8 with the boundary conditions in Eq. 9, one can show that

$$R_{\text{part}} = -\left(\frac{\partial U}{\partial c_2}\right)\frac{R_2}{FD_2} \quad [16]$$

and

$$Y_s = -1 + \left[\frac{A_2R_2 + \tan(A_2R_2)}{q\tan(A_2R_2) - 1}\right] \quad [17]$$

where

Table I. Global input parameter for the battery impedance simulation.

Parameter	Value
SOC	70%
T	298 K
$i_{0,1}$	0.69×10^{-3} A/cm^2
κ	5.5×10^{-5} S/cm
$L_{\text{electrolyte}}$	0.01 cm

$$q = \frac{A_1 + A_2\tan(A_2R_1)\tan(A_1R_1)}{A_1\tan(A_2R_1) - A_2\tan(A_1R_1)} \quad [18]$$

Here $A_1 = \sqrt{(-j\omega/D_1)}$ and $A_2 = \sqrt{(-j\omega/D_2)}$.

Overall single particle impedance.— With Fig. 3 and Eq. 14, the overall single spherical intercalation particle can be determined as

$$Y = \frac{1}{Z_{\text{total}}} = \left[\frac{1}{\frac{Z_{\text{faradaic}}}{1 + j\omega C_{dl1}Z_{\text{faradaic}}} + R_{\text{film}} + \frac{R_{ct2}}{1 + j\omega R_{ct2}C_{dl2}}}\right] + j\omega C_{\text{film}} \quad [19]$$

R_{film}, the SEI resistance per unit area, can be determined analytically as

$$R_{\text{film}} = \rho d\frac{R_2}{(d + R_2)} \quad [20]$$

where ρ is the resistivity of the film and d its thickness. The capacity of the SEI can also be calculated analytically as

$$C_{\text{film}} = \frac{\varepsilon R_2^2}{d} \quad \text{provided } d \ll R_2 \quad [21]$$

provided $d \ll R_2$ when treated as a spherical capacitor. Here ε is the permittivity of the SEI. In our model, however, it has been assumed that the capacitor of the SEI is a variable input value, which can come from experimental data.

Single porous electrode impedance.— Following the work of Meyers et al.,[27] it can be shown that the total impedance of a single porous electrode is

$$Z_{\text{electrode}} = \frac{L_d}{\kappa + \sigma}\left[1 + \frac{2 + \left(\frac{\sigma}{\kappa} + \frac{\kappa}{\sigma}\right)\sinh(\nu)}{\nu\sinh(\nu)}\right] \quad [22]$$

Here L_d is the thickness of the electrode, κ the electrolyte conductivity, σ the electrode conductivity, and ν is defined as

$$\nu = L_d\left(\frac{\kappa\sigma}{\kappa + \sigma}\right)^{-1/2}\bar{Y}^{1/2} \quad [23]$$

with the admittance

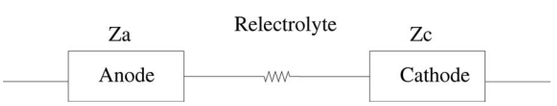

Figure 4. Equivalent-circuit diagram of the battery impedance. *Za* and *Zc* are the impedance of the anode and the cathode, respectively, and can be determined with Eq. 22.

Table II. Positive and negative electrode input parameters for the battery impedance simulation.

Parameter	Positive electrode	Negative electrode
a_s	33,120 cm^{-1}	79,200 cm^{-1}
L_d	0.01 cm	0.01 cm
σ	0.01 S/cm	0.05 S/cm
C_{dl1}	1×10^{-5} F/cm^2	1×10^{-5} F/cm^2
α_a	0.5	0.5
α_c	0.5	0.5
M_e	190 g/mol	89 g/mol
ρ_e	2.032 g/cm^3	1.62 g/cm^3
D_1	2.48×10^{-6} cm^2/s	1.0×10^{-11} cm^2/s
D_2	3.19×10^{-9} cm^2/s	1.0×10^{-12} cm^2/s
d	1.0×10^{-4} cm	1.0×10^{-4} cm
ρ	1.1×10^{7} Ω cm	1.1×10^{7} Ω cm
C_{film}	1.0×10^{-11} F/cm^2	1.0×10^{-11} F/cm^2
R_{ct2}	4.4 Ω cm^2	4.4 Ω cm^2
C_{dl2}	1.0×10^{-5} F/cm^2	1.0×10^{-5} F/cm^2
a_{g1}	8.0×10^{-4} cm	10.0×10^{-4} cm
a_{g2}	8.5×10^{-4} cm	10.5×10^{-4} cm
σ_{g1}	1.0×10^{-4} cm	1.0×10^{-4} cm
σ_{g2}	1.0×10^{-4} cm	1.0×10^{-4} cm

$$\bar{Y} = \text{NORM} \int_{r_2=0}^{\infty} 4\pi N(r_2) Y(r_1, r_2) r_2^2 dr_2 \quad [24]$$

The constant NORM in Eq 24 is introduced to ensure that after integration the correct interfacial surface area per unit volume, a_s, will be obtained

$$a_s = \text{NORM} \int_{r_2=0}^{\infty} 4\pi r_2^2 N(r_2) dr_2 \quad [25]$$

Here $N(r_2)$ is the particle distribution function, which is simply chosen as

$$N(r_2) = f(r_2) + g(r_2) \quad [26]$$

where $f(r_2)$ and $g(r_2)$ are both Gaussian distribution functions representing the two average grain sizes of the spherical particles. $Y(r_1,r_2)$ is the overall single particle admittance as determined in Eq. 19. Note that in Eq. 19 Y is a function of R_1 and R_2, while in Eq. 24 Y depends on the continuous parameters r_1 and r_2. Because it is assumed that the two different phases are homogeneous, r_1 and r_2 can be related to each other with the state of charge as $r_1 = \sqrt[3]{(SOC/100)} r_2$ and $r_1 = \sqrt[3]{1 - (SOC/100)} r_2$ for the positive and negative electrodes, respectively. R_{film} and C_{film} in Eq. 20 and 21 are functions of the radii R_1 and R_2 and can be transformed to be dependent on the continuous parameters r_1 and r_2. $R_{film}(r_2)$ and $C_{film}(r_1,r_2)$ can then be included in the $Y(r_1,r_2)$ term and integrated over the interfacial surface area per unit volume electrode as in Eq. 24. Here, however, we have taken a constant average value for $R_{film}(r_2)$, which is calculated as

$$R_{film}(r_2) = \rho d \frac{\bar{R}_2}{(d + \bar{R}_2)} \quad [27]$$

where $\bar{R}_2$ is chosen to be equal to the average of the mean values of the Gaussian distribution functions $f(r_2)$ and $g(r_2)$. Here $C_{film}(r_1,r_2)$ is also considered to be an variable input parameter, which can be obtained from experiments.

Table III. Fit parameters of the 4th polynomial function describing the voltage profile of the cathode and anode material.

Parameter	Positive electrode	Negative electrode
a_0	4.0481	1.3360
a_1	−2.3382	−15.7800
a_2	3.0632	57.2790
a_3	−0.1796	−79.0647
a_4	−2.0051	36.3895

Battery impedance.— Since the electrolyte impedance is determined by drift of ions, the total battery impedance can be obtained by simply considering the anode and the cathode to be in series with a resistor representing the impedance of the electrolyte (see Fig. 4). The total battery impedance can thus be written as

$$Z_{battery} = Z_a + Z_c + R_{electrolyte} \quad [28]$$

$R_{electrolyte}$ is determined from the conductivity (κ) and the thickness ($L_{electrolyte}$) of the electrolyte as

$$R_{electrolyte} = \frac{L_{electrolyte}}{\kappa} \quad [29]$$

Results and Discussion

The mathematical model developed in the previous section has been used to perform impedance simulations of a lithium-ion cell. In the simulations only the input parameters of the positive electrode were varied in order to investigate its influences on the total battery impedance. In Tables I-III the input parameters are presented for a battery impedance simulation. In Table II, a_{g1} and a_{g2} are the mean values of the Gaussian distribution functions $f(r_2)$ and $g(r_2)$, respectively, and σ_{g1} and σ_{g2} are their respective widths of the Gaussian distribution. Table III lists the fit parameters of the 4th polynomial function describing the voltage profile for the cathode and anode material, respectively. The influences of the state of charge, Li^+ diffusion coefficient, SEI, and particle size distribution on the battery impedance has been investigated.

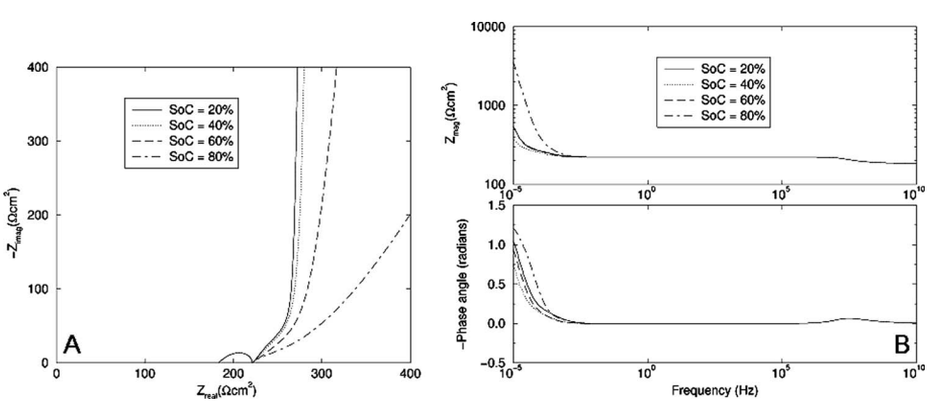

Figure 5. (A) Complex plane and (B) phase angle as a function of state of charge.

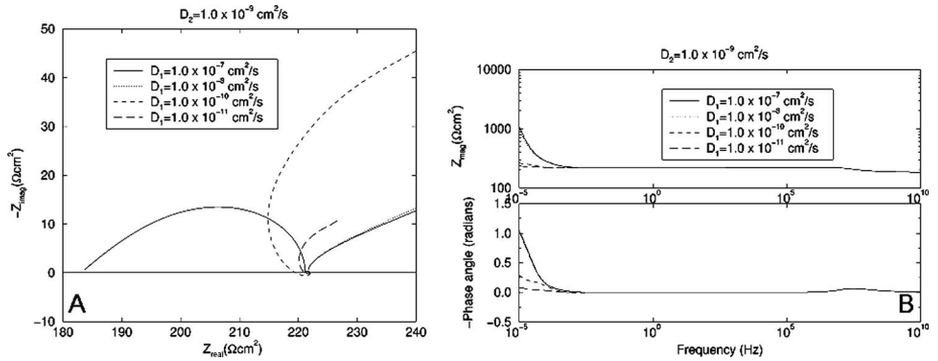

Figure 6. (A) Complex plane graph and (B) phase angle as a function of the Li^+ diffusion coefficient of the two different phases.

State of charge.— Simulations were performed where the state of charge of the battery has been varied between 20 and 80%. In Fig. 5 the complex plane graph, its magnitude, and the phase angle are shown as a function of the state of charge. The other input parameters are kept constant as given in Tables I and II. Changing the state of charge has two direct consequences on two implicit parameters of the simulation model. The $-[\partial U(x_0)/\partial x]$ term and the relationship between r_1 and r_2 are being changed. If the charge/discharge curve is considered to be linear, at least between a state of charge of 20 and 80%, then the $[-\partial U(x_0)/\partial x]$ should remain constant. However, since in our model the charge/discharge has been fitted to a 4th degree polynomial, the first derivative is not simply a constant. Nevertheless, the fluctuations stay within acceptable limits. The relationship between r_1 and r_2 are described by $r_1 = \sqrt[3]{(SOC/100)}r_2$ and $r_1 = \sqrt[3]{1-(SOC/100)}r_2$ for the positive and negative electrode, respectively. It can be easily seen that for the positive electrode r_1 will increase if the state of charge increases. The opposite will happen for the negative electrode. As a result we can see in Fig. 5A that the impedance is being lowered for low frequencies, when the state of charge increases. Both terms that are being changed by the state of charge are related to the diffusion impedance component (see Fig. 3), which describes the diffusion of the Li^+ ions in the spherical particles. The diffusion time constants we are dealing with here are typically in the order of seconds or higher, and therefore, contribution to the impedance spectrum can be expected only at frequencies say below 1 Hz. For high frequencies the impedance eventually becomes purely real, because the capacitor of the solid electrolyte shorted the electronic circuit as depicted in Fig. 3. The high-frequency resistance is then equal to the electrolyte resistance, e.g., in our case about 180 Ω.

Li^+ diffusion coefficient.— Figure 6 displays the complex plane, magnitude, and phase angle of a battery simulation for different Li^+ diffusion coefficients in the two phases of the positive electrode. The state of charge was set to 70% and the rest of the input parameters were kept constant. An apparent inductive loop can be seen which is the result of the difference in the diffusion coefficient in the two different phases. The loop is significant when $D_1 < D_2$. For $D_1 = 1.0 \times 10^{-10}$ cm^2/s, it can be clearly seen that the complex plane graph has also negative imaginary values. In Fig. 6, the change of the phase from 0.5π to 0.0π (resitance–capacitance behavior) at low frequencies is less visible if $D_1 \ll D_2$, which confirms a different behavior of the complex plane graph.

An inductive loop calculated with the simulations here has been observed in real cells by Song et al.,[31] Gnanaraj et al.,[32] and Itagaki et al.[33] Song et al. explained the inductive loop by an adsorption process during lithium intercalation. They further concluded that their findings were consistent with the finding of Takasu et al.,[34] who found lithium atoms to undergo Faraday adsorption on the surface. Gnanaraj et al. attributed the inductive loop to the formation of a concentration cell near the surface, where the electrons flow in an opposite direction compared to the Li ion migration. Although both of these explanations may seem different, a concentration cell may be found with adsorption as well. Nanosurface analysis on these systems then should give evidence where the Li ions reside and in what direction they move, hence to decide whether the inductive loop can be explained by adsorption or absorption of Li ions.

Clearly, by a change in the diffusion coefficients as a result of aging during the lifetime of a cell, a change in the overall measured impedance can be expected. This change is observed with a very characteristic behavior, and therefore, from impedance data on real cells, such a change in the impedance can then easily be attributed to a change in the diffusion coefficients.

Solid electrolyte interface.— The SEI thickness has been varied between 1.0 and 4.0 μm. The complex plane graph is shown in Fig. 7A. The phase angle and magnitude graph is displayed in Fig. 7B. Because the resistor of the SEI is really pure, in the complex plane plot it results in a wider arc when the SEI film thickness increases. For low frequencies the complex plane graph remained the same

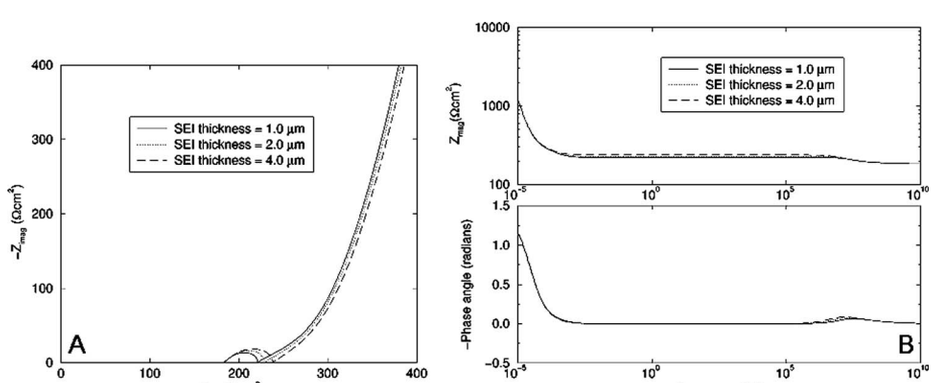

Figure 7. (A) Complex plane graph and (B) phase angle as a function of SEI thickness.

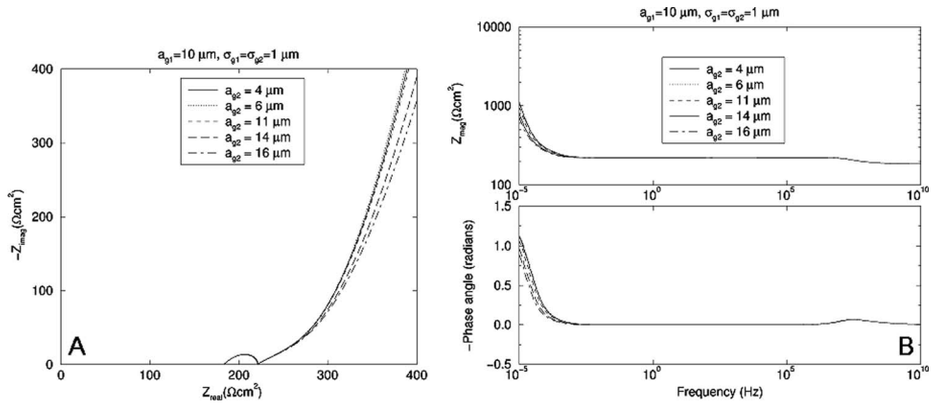

Figure 8. (A) Complex plane graph and (B) phase angle as a function of the mean value of the grain sizes of the particles.

except for the shift in the real axis as discussed above. The steepness of the complex plane graph for low frequencies is constant as the thickness, and thus, the SEI resistance increases. Due to the accepted nature of the SEI, i.e., charge transport is ohmic, the behavio of the diffusion part, i.e., at low frequencies, is not dependent on the SEI layer thickness (see Fig. 7).

As expected, a change in the SEI layer thickness as a result of aging may lead mainly to a shift of the touchdown of the arcs; an increase in the SEI layer thickness leads to an increase of the overall impedance. Hence, this aging aspect is reflected in the impedance only by a shift in the touchdown of the arcs.

Particle size distribution.— Finally, the influence of the particle size distribution on the battery impedance has been calculated with this model. The particle size distribution is dependent on the four parameters, a_{g1}, a_{g2}, σ_{g1}, and σ_{g2}, of the Gaussian distribution functions $f(r_2)$ and $g(r_2)$. First, the mean value a_{g2} was varied while $a_{g1} = 10.0$ μm, and their distributions, $\sigma_{g1} = \sigma_{g2} = 1.0$ μm, were kept constant. From the complex plane graph (Fig. 8), it can be seen that the impedance tail at low frequencies decreases if the difference between the mean values a_{g1} and a_{g2} increases. A similar effect is observed when the Gaussian deviation or width, σ_{g1} and σ_{g2}, are both increased at the same time (Fig. 9). At high frequencies the particle size distribution function does not seem to have a large influence on the impedance. This is because the particle size distribution influences only the diffusion impedance component, which describes the diffusion of the Li^+ ions. Varying the particle sizes means a variation of the diffusion length and thus, the low-frequency impedance. The diffusion impedance component is being shorted for high frequencies by the SEI capacitance, C_{film}, and the first double-layer capacitor, C_{dl1}, the diffusion part of ions in the particles.

Hence, by a change in the particle size and/or particle size distribution as a result of aging, a possible difference is observed only in the low frequency range.

Conclusions

A semimathematical model has been developed to simulate the impedance of a rechargeable battery. The battery is assumed to consist of only porous electrodes with spherical Li^+ intercalation particles. The particles are considered to have two distinct homogeneous phases due to charge and discharge. The diffusion of the Li^+ ions in the particles is described mathematically by solving the diffusion equation. The SEI and the electrolyte are described by passive electronic elements. First the model was developed for a single Li^+ intercalation particle. Using a Gaussian particle distribution and porous electrode theory, the model was applied to simulate the total impedance of a rechargeable lithium-ion battery.

This model was used to investigate the influence of the state of charge, Li^+ diffusion coefficient, SEI, and particle distribution on the total impedance of a lithium-ion battery. Particular attention was given to the positive electrode. The parameters of the negative electrode and the electrolyte were therefore kept constant in all simulations.

The simulation results have shown that the state of charge, which determines the relationship between the radii of the two distinct phases, has an effect only on the impedance for low frequencies. The impedances apparently decrease as the state of charge increases. The difference in Li^+ diffusion coefficient in the two phases gives an inductive loop in the complex plane graph. This loop is large if $(D_1 = 1.0 \times 10^{-10}\ \text{cm}^2/\text{s}) < (D_2 = 1.0 \times 10^{-9}\ \text{cm}^2/\text{s})$. Because the SEI impedance is purely resistive, an increase of its thickness results only in a shift of the arc along the real axis. Finally, we tested the influence of the particle distribution on the impedance by varying the mean values and deviation or width of the Gaussian particle distribution functions. The results show that if the difference between the mean values of the two main average grain sizes of the particles becomes larger the impedance will also decrease. Similar effects were found for the case when the deviation of the Gaussian distribution increases. The effects were, however, only visible at low

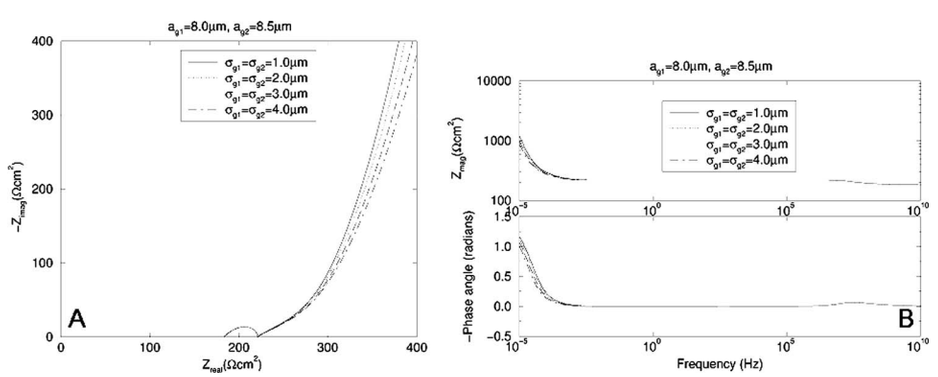

Figure 9. (A) Complex plane graph and (B) phase angle as a function of the width of the Gaussian particle distribution.

frequencies where diffusion of Li^+ ions occurs. Modifying the particle size distribution function results in a change of the diffusion length. The particle size distribution function is therefore related to the impedance component *Z*, which describes the diffusion process and is being shorted at high frequencies. Hence, by the variations in the measured impedances during the lifetime of a cell and comparing it with simulations it is possible to conclude what sort of aging mechanism is responsible for the fading of the cell.

Acknowledgments

This work has been carried out through European Commission supported project "LIBERAL" under contract number ENK6-CT2002-00626. Professor S. W. de Leeuw, Professor J. Schoonman, and Dr. J. Heringa are kindly acknowledged for fruitful discussions. The Delft Research Centre for Sustainable Energy "SENECU" is thanked for additional financial support.

Delft University of Technology assisted in metting the publication costs of this article.

References

1. J. Vetter, P. Novák, M. R. Wagner, C. Veit, K.-C. Möller, J. O. Besenhard, M. Winter, M. Wohlfahrt-Mehrens, C. Vogler, and A. Hammouche, *J. Power Sources*, To be published.
2. D. P. Abraham, J. Liu, C. H. Chen, Y. E. Hyung, M. Stoll, N. Elsen, S. MacLaren, R. Twesten, R. Haasch, E. Sammann, I. Petrov, K. Amine, and G. Henriksen, *J. Power Sources*, **119–121**, 511 (2003).
3. I. Bloom, S. A. Jones, V. S. Battaglia, G. L. Henriksen, J. P. Christophersen, R. B. Wright, C. D. Ho, J. R. Belt, and C. G. Motloch, *J. Power Sources*, **124**, 538 (2003).
4. D. P. Abraham, S. D. Poppen, A. N. Jansen, J. Liu, and D. W. Dees, *Electrochim. Acta*, **49**, 4763 (2004).
5. K. Mizushima, P. C. Jones, P. J. Wiseman, and J. B. Goodenough, *Mater. Res. Bull.*, **15**, 783 (1980).
6. J. R. Dahn, U. von Sacken, and C. A. Michal, *Solid State Ionics*, **44**, 87 (1990).
7. R. Kanno, H. Kubo, Y. Kawamoto, T. Kamiyama, F. Izumi, Y. Takeda, and M. Takano, *J. Solid State Chem.*, **110**, 216 (1994).
8. T. Ohzuku, A. Ueda, and M. Nagayama, *J. Electrochem. Soc.*, **140**, 1862 (1993).
9. M. E. Arroyo y de Dompablo and G. Ceder, *J. Power Sources*, **119–121**, 654 (2003).
10. E. Antolini, *Solid State Ionics*, **170**, 159 (2004).
11. J. Barker, R. Koksbang, and M. Y. Saidi, *Solid State Ionics*, **89**, 25 (1996).
12. W. Ebner, D. Fouchard, and L. Xie, *Solid State Ionics*, **69**, 238 (1994).
13. W. Li, J. N. Reimers, and J. R. Dahn, *Solid State Ionics*, **67**, 123 (1993).
14. B. Zachau-Christiansen, K. West, and T. Jacobsen, *Solid State Ionics*, **9/10**, 399 (1983).
15. I. Saadoune and C. Delmas, *J. Solid State Chem.*, **1998**, 136.
16. C. S. Johnson and A. J. Kropf, *Electrochim. Acta*, **47**, 3187 (2002).
17. M. D. Levi, K. Gamolsky, D. Aurbach, U. Heider, and R. Oesten, *J. Electroanal. Chem.*, **477**, 32 (1999).
18. M. D. Levi, K. Gamolsky, D. Aurbach, U. Heider, and R. Oesten, *Electrochim. Acta*, **45**, 1781 (2000).
19. J. Fan and P. S. Fedkiw, *J. Electrochem. Soc.*, **144**, 399 (1997).
20. R. Koksbang, I. I. Olsen, P. E. Tonder, N. Knudsen, and D. Fauteux, *J. Appl. Electrochem.*, **21**, 301 (1991).
21. C. D. Desjardins and K. Maclean, *J. Electrochem. Soc.*, **136**, 345 (1986).
22. F. Capuano, F. Croce, and B. Scrosati, *J. Electrochem. Soc.*, **138**, 1918 (1991).
23. G. Pistoia, A. Antonin, R. Rosati, and D. Zane, *Electrochemica*, **141**, 2683 (1996).
24. G. Montesperelli, P. Nunziante, M. Pasquali, and G. Pistoia, *Solid State Ionics*, **37**, 149 (1990).
25. M. Gasberscek and S. Pejovnik, *Electrochim. Acta*, **41**, 1137 (1996).
26. S. R. Narayanan, D. H. Shen, S. Surampudi, A. I. Attia, and G. Halpert, *J. Electrochem. Soc.*, **140**, 1854 (1993).
27. J. P. Meyers, M. Doyle, R. M. Darling, and J. Newman, *J. Electrochem. Soc.*, **147**, 2930 (2000).
28. V. Srinivasan and J. Newman, *J. Electrochem. Soc.*, **151**, A1517 (2004).
29. V. Srinivasan and J. Newman, *J. Electrochem. Soc.*, **151**, A1530 (2004).
30. M. D. Levi and D. Aurbach, *J. Phys. Chem. B*, **108**, 11693 (2004).
31. J. Y. Song, H. H. Lee, Y. Y. Wang, and C. C. Wan, *J. Power Sources*, **111**, 255 (2002).
32. J. S. Gnanaraj, R. W. Thompsen, S. N. Iaconatti, J. F. DiCarlo, and K. M. Abraham, *Electrochem. Solid-State Lett.*, **8**, A128 (2005).
33. M. Itagaki, N. Kobari, S. Yotsuda, K. Watanabe, S. Kinoshita, and M. Ue, *J. Power Sources*, **135**, 255 (2004).
34. R. Takasu, K. Sekine, and T. Takamura, *J. Power Sources*, **81–82**, 224 (1999).